The Astrophysical Journal Letters, 808:L16 (5pp), 2015 July 20 doi:10.1088/2041-8205/808/1/L16

FAINT LUMINESCENT RING OVER SATURN'S POLAR HEXAGON

Alberto Adriani[1], Maria Luisa Moriconi[2], Emiliano D'Aversa[1], Fabrizio Oliva[1], and Gianrico Filacchione[1]
[1] Institute of Space Astrophysics and Planetology of INAF, Via Fosso del Cavaliere 100, I-00133 Rome, Italy; alberto.adriani@iaps.inaf.it
[2] Institute of Atmospheric Sciences and Climate of CNR, Via Fosso del Cavaliere 100, I-00133 Rome, Italy
Received 2015 January 28; accepted 2015 June 14; published 2015 July 20

ABSTRACT

Springtime insolation is presently advancing across Saturn's north polar region. Early solar radiation scattered through the gaseous giant's atmosphere gives a unique opportunity to sound the atmospheric structure at its upper troposphere/lower stratosphere at high latitudes. Here, we report the detection of a tenuous bright structure in Saturn's northern polar cap corresponding to the hexagon equatorward boundary, observed by Cassini Visual and Infrared Mapping Spectrometer on 2013 June. The structure is spectrally characterized by an anomalously enhanced intensity in the 3610–3730 nm wavelength range and near 2500 nm, pertaining to relatively low opacity windows between strong methane absorption bands. Our first results suggest that a strong forward scattering by tropospheric clouds, higher in respect to the surrounding cloud deck, can be responsible for the enhanced intensity of the feature. This can be consistent with the atmospheric dynamics associated with the jet stream embedded in the polar hexagon. Further investigations at higher spectral resolution are needed to better assess the vertical distribution and microphysics of the clouds in this interesting region.

Key words: infrared: planetary systems – instrumentation: spectrographs – methods: data analysis – planets and satellites: atmospheres – radiative transfer – techniques: imaging spectroscopy

1. INTRODUCTION

Saturn's north pole has been the object of many studies and observations since the *Voyager* infrared images revealed for the first time its hexagonal-shaped vortex circulation (Godfrey 1988). The Cassini mission added much more information about the atmospheric structure and composition (Baines et al. 2009; Sánchez-Lavega et al. 2014) since its arrival at Saturn. However, as the Saturn Orbit Insertion of the Cassini spacecraft has occurred during the winter season of the northern hemisphere, the first years of the mission have been suitable for studying the northern regions of the atmosphere only through thermal emission at near- and mid-infrared wavelengths (Fletcher et al. 2008) or through fluorescence connected to the auroral emissions (Melin et al. 2011), whose contrast appears enhanced in low solar elevation conditions. In this Letter, we analyze a specific polar hexagon observation acquired by the Visual and Infrared Mapping Spectrometer (VIMS) infrared channel during a polar orbit hovering over the grazing-illuminated polar cap moving from the night side toward the Sun.

2. OBSERVATIONS

A tenuous bright structure has been detected over Saturn's north pole on 2013 June 25 by Cassini's VIMS (Brown et al. 2004), approximately coincident with the hexagon-shaped polar jet (Allison et al. 1990). The remarkably high 1 s exposure time of this observation, though saturating a portion of the spectrum over the planet day side, is particularly suitable for the detection of small spectral signatures. In particular, the feature appears as an anomalously high signal around 2500 nm and in the 3600–3730 nm range. The latter is spectrally shaped as a double peak with maxima at 3665 and 3700 nm. Our very first hypothesis of a possible auroral emission had to be discarded due to its hexagonal shape, the lack of other spectral signatures typical of the H_3^+ emissions between 3 and 4 μm (Connerney & Satoh 2000), and the amplitude of the signal at 2500 nm that is two orders of magnitude higher than the one expected by an auroral emission.

In Figure 1 (left panel), we show a red giant branch color-composite image taken from the VIMS cube V1753141911 by selecting wavelengths corresponding to the 3665 and 3700 nm (doublet peaks) and thermal emission in the 5000 nm region in order to enhance the shape of the bright structure. The latitudinal coverage and spatial resolution of the observation is given by the polar map projection of the same image shown in the right panel of Figure 1. The latitude values used in the map and hereafter in the text are calculated in the planetocentric coordinate system. The bright structure is latitudinally coincident with the equatorward boundary of the hexagon, a region where the thermal emission from the deep atmosphere is strongly absorbed by optically thick tropospheric clouds.

The spatial average spectrum of the hexagonal bright structure is shown in Figure 2 for the 1700–3800 nm range, where our analysis is focused, together with the spectra averaged over the inner polar, the planetary limb (100–300 km above the 1 bar pressure level), and the night-side regions. The radiance values in the plots are obtained from the raw data by using the radiometric calibration pipeline described in Filacchione et al. (2012). The shape of the doublet spectral feature is recognizable in all the spectra of the illuminated hemisphere of the planet, though very faint, but it is significantly more intense only over the hexagon. In Figure 2, each spectrum is color-coded according to the corresponding region as it appears from the associated image. In order to exclude the bright structure belonging to an infrared auroral emission, Figure 2 also shows an infrared H_3^+ auroral emission spectrum for comparison, observed during a different orbit (cube V1595126852). This spectrum is also a spatial average, calculated over the main auroral oval region. The comparison shows the absence of the many H_3^+ spectral signatures as well as the energy difference between the auroral emission and the bright structure. The spatial distribution of the auroral emission at 3530 nm (one of the most prominent H_3^+ emission lines) can

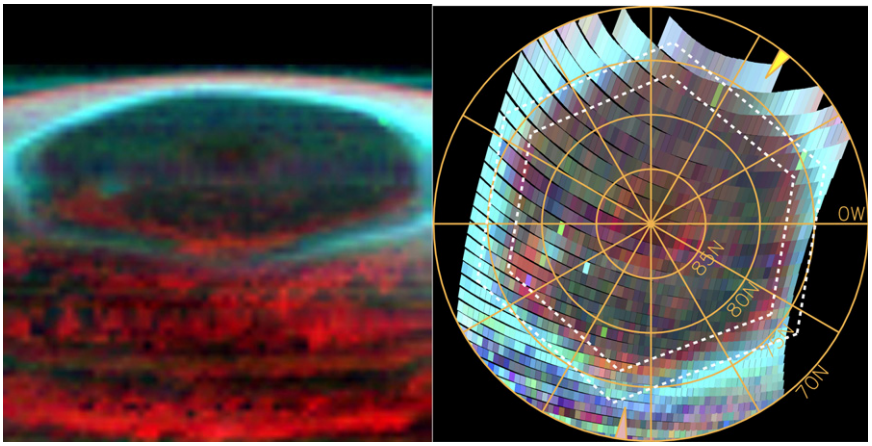

Figure 1. Left panel: an anomalously bright structure along the northern polar hexagon shown in an RGB color-composite image. Red channel maps the intensity of thermal emission (taken at 4867 nm), whereas green and blue channels map the 3665 and 3700 nm wavelength, respectively (doublet's peaks). Right panel: the same RGB image in a polar projection map, showing latitudinal coverage (planetocentric) and spatial resolution of the observation, as well as the position of the polar hexagon (dashed white lines) taken from Sánchez-Lavega et al. (2014). Arrows indicate the viewing (bottom, pink arrow) and illumination (top right, yellow arrow) directions.

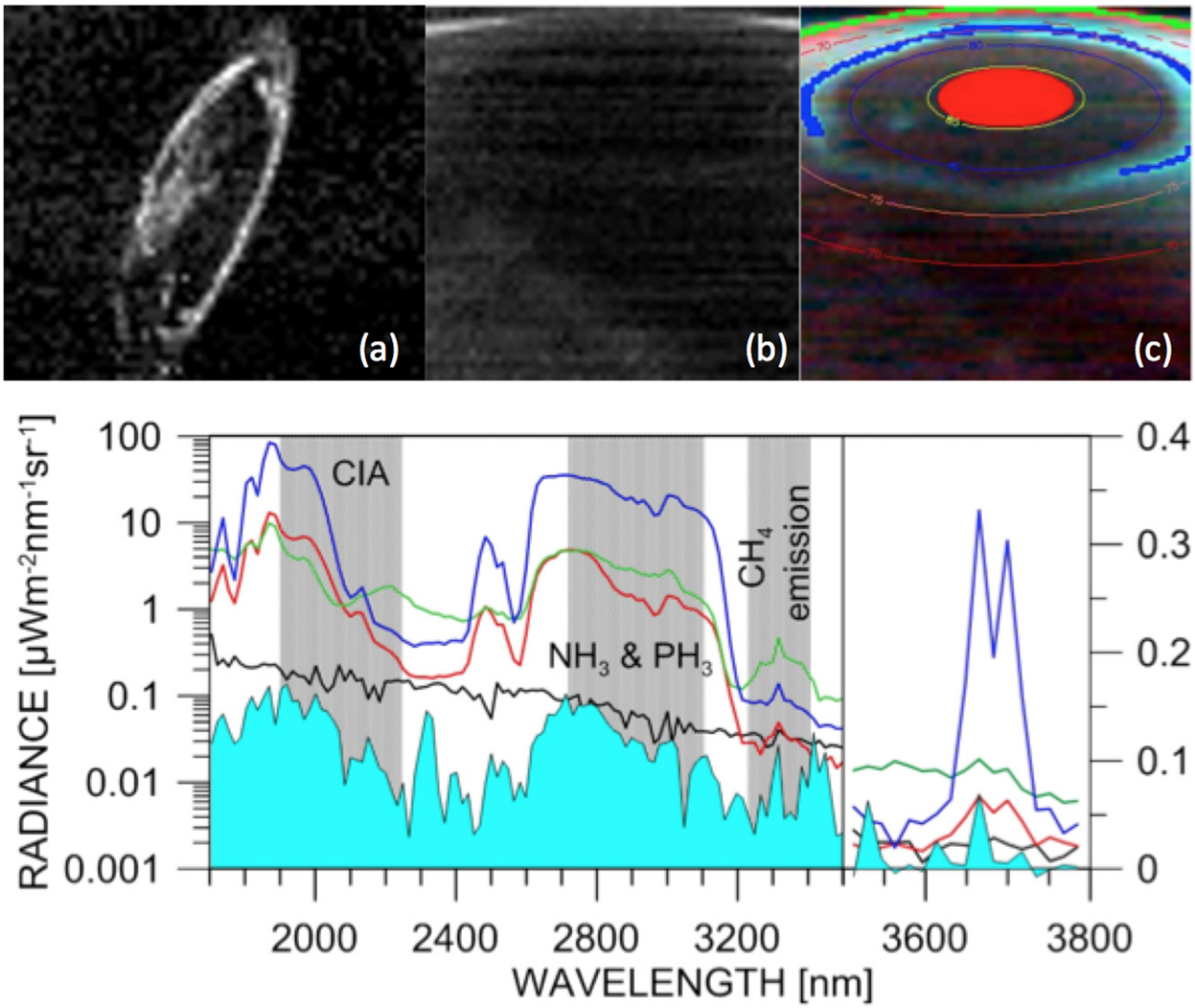

Figure 2. Spectral comparison in the polar region, from the same data cube shown in Figure 1. Bottom panel: the blue curve is an average spectrum over the bright hexagon feature, showing a very intense 3700 nm doublet; the green curve is a planetary limb average spectrum showing the typical 3300 nm methane emission complex; the red curve is an average spectrum taken over the central polar region; the black curve is an average spectrum from the dark side of the planet; the light blue shaded curve is a Saturn aurora spectrum (taken from panel (a)) shown for comparison of emission features. Refer to panel (c) to locate the actual averaging regions for the blue, red, and green spectra. Note the different axis scale used to enhance the 3700 nm doublet feature. Panels (a) and (b) are monochromatic at the same wavelength (3530 nm) from a cube showing a typical aurora (image (a)) and cube here under study. Panel (c) shows an RGB color-composite image similar to that of Figure 1, where the red thermal wavelength (4867 nm) has been replaced with the CH_4 Q branch at 3333 nm.

be appreciated in Figure 2(a), while the image at the same wavelength in the observation under study (Figure 2(b)) shows the absence of any auroral signature.

The variation of the doublet's intensity with the illumination angle and the comparison with the limb spectrum (showing the 3.3 μm methane emission) suggest that the doublet is a true reflectance feature of the atmosphere. As shown in Figure 2, the doublet signature does not appear in the average spectrum taken on the planet's night side (black curve in Figure 2).

3. DATA ANALYSIS

A search for the existence of the doublet spectral feature has been carried out in several VIMS data, but a spectral doublet feature of such high intensity has only been found in recent observations of the equatorial zone and the northern polar cap. The feature is located in a region of the Saturn near-infrared spectrum where methane absorption is strong and its detection requires high exposure times to overcome the noise level. Furthermore, the anomalously high brightness is observable only at relatively high solar phase angles (128° for the observation discussed here). This indicates that the enhanced reflectivity could be ascribed to forward-scattering particles, probably comparable in size to the order of magnitude of the wavelength.

From the spectral point of view, the doublet is located between two very strong methane absorption bands at 3.3 and 3.8 μm, and it represents a relatively weak transparency window of atmospheric transmission. The hexagonal shape of the structure suggests that it originates at tropospheric altitudes: in fact, the temperatures retrieved in Saturn polar regions from data by the Composite Infrared Spectrometer on board Cassini (Fletcher et al. 2008, 2015) showed a circular stratospheric thermal field, not giving any hint of a possible hexagonal shape. Even stellar occultation data from VIMS at high latitude do not observe any 3700 nm doublet signature in the stratosphere (Kim et al. 2012).

In order to reproduce the observed spectra, we used a plane-parallel multiple-scattering line-by-line radiative transfer model (Colosimo et al. 2010; Oliva et al. 2013, 2014, 2015), based on the DISORT solver (Stamnes et al. 1988). We took into account only methane as absorbing gas, with molar fractions of different isotopes from Fletcher et al. (2007, 2009), absorption coefficients derived from the HITRAN 2012 database (Rothman et al. 2013), whereas the thermal profile is taken from Lindal (1992). The cloud vertical structure consists of two particulate layers, one in the lower stratosphere and the other in the upper troposphere (see Table 1). The grain size distributions are assumed as lognormal for the stratospheric layer and as modified-gamma (Hansen 1971) for the tropospheric one. Both layers are made of the gray component described in Karkoschka & Tomasko (2005). We limited our calculations to those ranges where the spectrum is unsaturated and not sensitive to gases other than methane. Thus, as shown in Figure 3, we exclude spectral ranges dominated by non-LTE emissions and absorptions by hydrogen, helium (collision-induced absorption), phosphine, and ammonia.

As illustrated in Figure 3, we were able to fit spectra both in and out of the observed structure by changing the vertical clouds structure. Synthetic spectra are mostly sensitive to the top pressure of the tropospheric cloud, its optical thickness, and the stratospheric cloud optical thickness. We were not able to constrain the top pressure of the stratospheric cloud above 0.5 hPa and the base pressure of the tropospheric one below 700 hPa. Table 1 reports the best-fit values we obtained, even if equally reliable fits can be achieved by changing the vertical extension of the clouds and adjusting the other parameters.

We also point out that the methane correlated-k coefficients provided by Sromovsky et al. (2012) and the band model by Karkoschka & Tomasko (2010) were unable to reproduce the doublet methane feature, possibly leading to erroneous assignments of this spectral feature due to molecules other than methane. We were able to fit the spectra only using a line-by-line approach referring to the HITRAN 2012 database.

Table 1
Cloud Layers Characteristics Used in the Best-fitting Simulation

		Off-bright Feature (pixel 1–35)	On-bright Feature (pixel 3–36)
	Incidence Angle	72.6°	72.4°
	Emission Angle	58.8°	59.3°
	Solar Phase Angle	128.0°	128.0°
Stratospheric Haze	Size Distribution	Lognormal	Lognormal
	$r_{\rm eff}$, $v_{\rm eff}$	0.25 μm, 0.2	0.25 μm, 0.2
	Top Pressure	<0.5 hPa	<0.5 hPa
	Bottom Pressure	114 ± 11 hPa	95 ± 9 hPa
	Optical Depth	0.006 @ 2 μm	0.006 @ 2 μm
Tropospheric Haze	Size Distribution	Gamma	Gamma
	$r_{\rm eff}$, $v_{\rm eff}$	1.65 μm, 0.2	1.65 μm, 0.2
	Top Pressure	114 ± 11 hPa	95 ± 9 hPa
	Bottom Pressure	>700 hPa	>700 hPa
	Optical Depth	4.9 @ 2 μm	4.9 @ 2 μm

Note. $r_{\rm eff}$ and $v_{\rm eff}$ are the effective radius and variance of the particle size distribution, respectively.

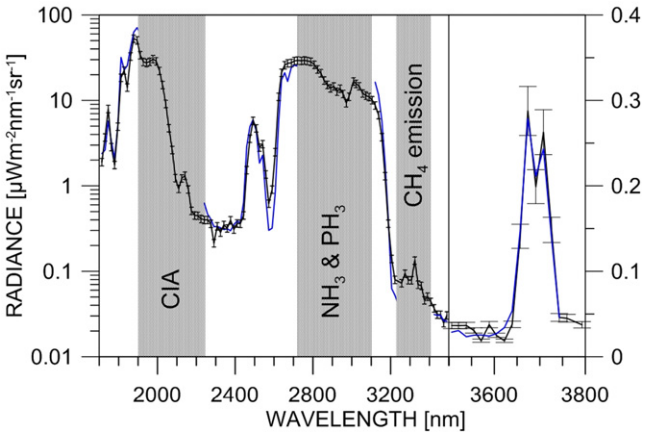

Figure 3. Best-fitting result for a spectrum on the bright hexagon feature; measured radiance is shown in black, synthetic spectrum in blue; shaded in gray: spectral zones excluded from the simulations due to the presence of ammonia, phosphine, hydrogen collision-induced absorption, and methane emission (see the text); error bars account for an error of ±10% on the measured spectrum.

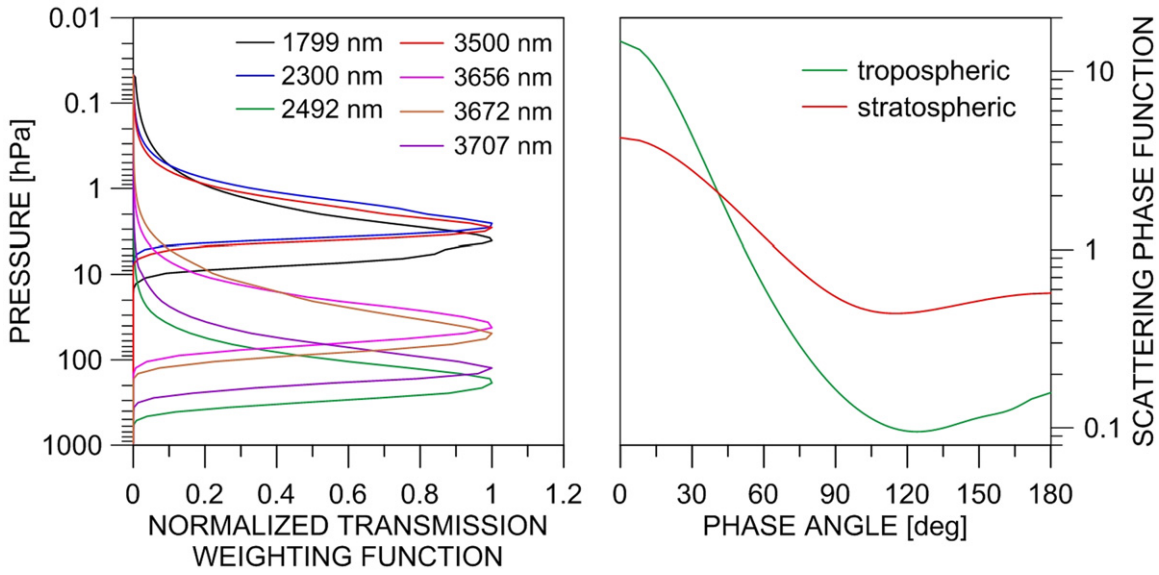

Figure 4. Left panel: transmission weighting functions in clear sky computed from the atmospheric model described in the text. Right panel: single-scattering phase functions at 3707 nm relative to the best-fitting grain size distribution of the two cloud layers used in the model.

The transmission weighting functions of the atmosphere in clear sky conditions (Figure 4, left panel) give an indication of the atmospheric altitudes probed by the selected VIMS channels. As mentioned above, the doublet's wavelengths and the 2500 nm wavelength are mostly sensitive to the properties of the tropospheric cloud, whereas the wavelengths around 1800, 2300, and 3500 nm are diagnostic of the lower stratosphere. This is consistent with the preliminary results we have obtained (Table 1) indicating that the variation of altitude of the tropospheric cloud is the key parameter to describe the observed feature. Hence, the enhanced intensity of the doublet can be explained by the rising of the tropospheric cloud by about 5–10 km (15%–30% of the scale height). The fact that the doublet appears weaker in other VIMS observations can be related to the different phase angles. In fact, in order to obtain the abovementioned fits at the high phase angle of the investigated observation, we had to use strong forward-scattering cloud particles (Figure 4).

The region of the polar hexagon, where the high reflection feature is located, straddles the polar jet stream, whose wind velocities peak at about 76N, with a latitudinal variation of about 1.5° due to the non-axisymmetric nature of the hexagon (Baines et al. 2009). The bright feature is about 2° south of the jet and is very close in latitude to a maximum of the jet curvature (Sánchez-Lavega et al. 2014). Jet streams are usually associated with vertical motions, and the rising air can easily produce condensation due to adiabatic cooling. Moreover, the upwelling from lower altitudes can produce accumulation of particles and trace gases advected from deeper tropospheric layers at mid-latitudes increasing the vertical mixing of gases. On the other hand, the rising air supplying the polar jet can introduce condensation nuclei in the upper troposphere and enhance local haze formation from local trace gases present there. Mixing with the air coming from below should be supported by the turbulence produced by the jet stream shear with the surrounding air. The formation of particles can increase the atmospheric optical thickness as well as the efficiency in blocking the thermal emission from below. Among the molecule candidates for condensation there are aldehydes—functional group H – C = O—and methanol that, even if never detected on Saturn, are predicted by some chemical models (Moses et al. 2000) in Saturn's lower stratosphere and upper troposphere and eventually condensate if abundant enough.

4. CONCLUSIONS

We described an anomalously bright feature in Saturn's northern polar hexagon, as recently observed by VIMS in high phase geometry. In particular, the brightness anomaly is observed at wavelengths around 3700 nm, where the methane absorption at VIMS resolution is shaped as a double peak. We were able to accurately reproduce the variation of Saturn's spectrum at the wavelengths of interest, showing their sensitivity to the atmospheric structure in the upper troposphere–lower stratosphere (UTLS). Simulations performed using either the methane correlated-k coefficients provided by Sromovsky et al. (2012) or the band model by Karkoschka & Tomasko (2010) failed in reproducing the doublet methane feature; thus, we suggest using HITRAN 2012 coefficients in this range. Our first results suggest that a strong forward scattering by a tropospheric cloud with a higher top in respect to the surrounding cloud deck can be responsible for the enhanced intensity of the feature. This can be consistent with the atmospheric dynamics associated with the jet stream embedded in the polar hexagon and compatible with an increased abundance of particulates suggesting ongoing condensation and/or advection.

Further investigation of the doublet feature with higher spectral and spatial resolution will be necessary to more deeply assess the nature of the scattering particles. However, this study, even at the present VIMS resolution, gives clues about the atmospheric structure of the UTLS region over Saturn's north pole.

This work has been developed thanks to the financial support of the Italian Space Agency.

REFERENCES

Allison, M., Godfrey, D. A., & Beebe, R. F. 1990, Sci, 247, 1061
Baines, K. H., Momary, T. W., Fletcher, L. N., et al. 2009, P&SS, 57, 1671
Brown, R. H., Baines, K. H., Bellucci, G., et al. 2004, SSRv, 115, 111
Colosimo, S. F., D'Aversa, E., Adriani, A., et al. 2010, in EGU General Assembly 2010 (Göttingen, Germany: Copernicus)
Connerney, J. E. P., & Satoh, T. 2000, RSPTA, 358, 2471
Filacchione, G., Capaccioni, F., Ciarniello, M., et al. 2012, Icar, 220, 1064
Fletcher, L. N., Irwin, P. G. J., Orton, G. S., et al. 2008, Sci, 319, 79
Fletcher, L. N., Irwin, P. G. J., Sinclair, J. A., et al. 2015, Icar, 250, 131
Fletcher, L. N., Irwin, P. G. J., Teanby, N. A., et al. 2007, Icar, 188, 72
Fletcher, L. N., Orton, G. S., Teanby, N. A., et al. 2009, Icar, 199, 351
Godfrey, D. A. 1988, Icar, 76, 335
Hansen, J. E. 1971, JAS, 28, 1400
Karkoschka, E., & Tomasko, M. G. 2005, Icar, 179, 195
Karkoschka, E., & Tomasko, M. G. 2010, Icar, 205, 674
Kim, S. J., Sim, C. K., Lee, D. W., et al. 2012, P&SS, 65, 122
Lindal, G. F. 1992, AJ, 103, 967
Melin, H., Stallard, T., Miller, S., et al. 2011, GeoRL, 38, L15203
Moses, J. I., Lellouch, E., Bezard, B., et al. 2000, Icar, 145, 166
Oliva, F., Adriani, A., Liberti, G. L., et al. 2013, in ESPC 2013 (Göttingen, Germany: Copernicus) EPSC2013-158
Oliva, F., Adriani, A., Moriconi, M. L., et al. 2014, in 40th COSPAR Sci. Assembly (Moscow: COSPAR), poster TFS-S-172
Oliva, F., Adriani, A., Moriconi, M. L., et al. 2015, Icar, submitted
Rothman, L. S., Gordon, I. E., Babikov, Y., et al. 2013, JQSRT, 130, 4
Sánchez-Lavega, A., del Río-Gaztelurrutia, T., Hueso, R., et al. 2014, GeoRL, 41, 1
Sromovsky, L. A., Fry, P. M., Boudon, V., et al. 2012, Icar, 218, 1
Stamnes, K., Tsay, S. C., Wiscombe, W., et al. 1988, ApOpt, 27, 2502